STScI | SPACE TELESCOPE SCIENCE INSTITUTE

JWST TECHNICAL REPORT

Title: NIRISS Commissioning Results: NIRISS Single Object Slitless Spectroscopy Photometric Calibration	Doc #: JWST-STScI-008270, SM-12 Date: 19 October 2022 Rev: -
Authors: Kevin Volk and the NIRISS team Phone: 410-338-4409	Release Date: 2 November 2022

1.0 Abstract

The reduction of the NIRISS Single Object Slitless Spectroscopy photometric observations in commissioning is described in this report. Observations of the photometric standard star BD+60°1753 were used to derive the spectral response of the GR700XD grism mode of NIRISS in orders 1, 2, and 3. There are some uncertainties in the results due to issues with the spectral extraction from bad pixels, because of the tilt of the mono-chromatic PSF with result to the trace, and because the aperture corrections are difficult to derive for this observation mode and were not applied (hence the calibration derived is specific to the aperture used). All of these issues will need to be addressed further in cycle 1 calibration observations to improve the photometric calibration of the SOSS mode.

2.0 Introduction

The commissioning program NIS-017, APT program 1091, was devoted to the photometric calibration of the Single Object Slitless Spectroscopy (SOSS) mode. The program consists of a number of individual observations of a single target, the photometric standard star BD+60°1753, including a moderately long time series observation intended to give a first look at the photometric stability of NIRISS in this mode. The main goal of the program is to produce conversion factors from the observed spectral signal in ADU/s to output units of MJy in each of the three available orders for the spectra. The SOSS mode is unusual in that the monochromatic response is highly distorted by a weak cylindrical lens incorporated with the GR700XD grism, such that there is significant overlap between orders 1 and 2 at the longer wavelengths, above about 1.15 μm in second order and above about 2.3 μm in first order, with the effect of the overlap being much more of an issue for second order. One fundamental issue with the calibration of the SOSS mode is the question of separating the orders, which was not properly solved at the time of NIRISS commissioning. The highly distorted

monochromatic response, which will be denoted the "point spread function" (PSF) by analogy with normal imaging, also makes any attempt at aperture correction very difficult.

The target selected for the program, BD+60°1753, is a star of spectral type A0mA1V. This star is one of the well-established photometric standards listed on the CALSPEC pages (https://www.stsci.edu/hst/instrumentation/reference-data-for-calibration-and-tools/astronomical-catalogs/calspec; see Bohlin, Gordon & Tremblay (2014)) and was one of the primary photometric standards used for calibration of the Spitzer Space Telescope. The star has not been specifically calibrated as a spectrophotometric standard over the SOSS wavelength range, although part of this range is covered by observations of the star with the Hubble Space Telescope STIS instrument. The spectrum from STIS is available on the CALSPEC pages along with a stellar model spectrum matched to the STIS spectrum. A spectral type of A0mA1V is assigned from analysis of the STIS spectrum, denoting that the star has a mild Am characteristic with a weak Ca K line for the normal spectral type of A0V assigned from the Balmer lines and slightly enhanced metallic lines that would indicate a spectral type of A1V. The optical spectrum of this star from STIS is very strongly similar to that of Sirius which makes it an attractive star to use for SOSS photometric calibration since we know that Sirius does not suffer from the effects of fast rotation that make Vega somewhat difficult to model with a stellar atmosphere code. The spectral type of the star is given as A1V in SIMBAD (Wenger et al., 2000) citing the Spitzer IRAC photometric calibration paper of Reach et al. (2005). There is no specific mention as to the providence of the spectral type in that paper. No other spectral type references are given in SIMBAD. The star is bright enough (V=9.65) that it should have been part of the HD catalogue, but it has no entry therein.

3.0 Observations and Data Reduction

The SOSS observation of BD+60°1753 was taken on 5 June, 2022. A target acquisition observation in the F480M filter plus the CLEARP filter in the 64×64 pixel SUBTASOSS sub-array was carried out before any of the spectroscopic observations were done. The first observation used a series of different exposures of the star in SOSS mode with different sub-array and ramp configurations, with the GR700XS grism paired with the CLEAR element and then with the F277W blocking filter. The F277W observations were taken to separate out the first order spectrum in the longer wavelengths where there is more of an issue with the second order spectrum overlap. Observations were taken in SUBSTRIP256, SUBSTRIP96, and with full frame read-out for both configurations. These exposures ranged from 193 to 712 seconds in duration. A second observation was done immediately thereafter where the star was observed in the normal SOSS time series mode in SUBSTRIP256, first a normal CLEAR exposure of 3 frames per integration times 876 integrations and then a shorter exposure of 3 frames per integration times 40 integrations with the F277W filter in the beam. The integrations of the second observation took approximately 5.35 hours and 0.24 hours respectively. The photometric analysis was done using the second observation because it represents the

longest available exposure time in these two configurations, and hence the best signal-to-noise ratio (S/N).

The acquisition images for the star were photometrically reduced to produce imaging conversion values in (MJy/ster)/(ADU/s) for comparison with the other imaging photometric observations during NIRISS commissioning. The results were found to the consistent within about 2% with the other photometric observations in the F480M filter.

The SOSS mode observations were reduced in the JWST pipeline through level 1 to produce rate images and then flat-fielded, after which the spectral extraction was done using the "Algorithme de Traitement d'Ordres ContAmines" (ATOCA) routines developed by members of the NIRISS instrument team at the Université de Montréal for the JWST pipeline. Unfortunately, the ATOCA code did not produce the expected deblending of the orders in the NIRISS SOSS commissioning observations. The original expectation was that the code would separate orders 1 and 2 properly for the photometric calibration once a suitable set of reference files were produced based upon this observation and the wavelength calibration from program NIS-018/APT 1092. In the event although a specific set of reference files were produced for the wavelength and trace solutions specific to the BD+60°1753 observation by Loïc Albert the extraction did not operate as expected. The only "solution" was to extract the spectral orders using ATOCA without any attempt at deblending. This was done using the default aperture size of ±20 pixels from the trace position. Due to turning off the profile fitting and deblending parts of the ATOCA code, the extracted spectra also have no correction for bad pixels within the extraction aperture. This introduces additional noise in the extracted spectra at up to the few percent level from pixel to pixel. Currently the ATOCA code does not allow for the small tilt of the SOSS monochromatic PSF with respect to the pixel y axis, but extracts a fixed rectangular aperture in the y direction for each x pixel value along the trace.

For orders 2 and 3 the ATOCA spectra did not cover the full wavelength range but stopped at the minima in the response. In order to also extract the spectra at longer wavelengths than the minimum in second order and at shorter wavelengths than the minimum in third order the trace over these wavelengths was used with a simple box extraction to get the signal at these wavelengths. Since the ATOCA software was only doing a box extraction with no deblending this procedure is identical to what ATOCA would do if the trace were extended to the full range of the orders. The rectangular extraction spectra were used where the ATOCA extraction was not available, although for all of first order and the main parts of second and third orders were calibrated with the ATOCA spectrum.

The output mean rate image from the entire set of ramps is shown in Figure 1 below using a logarithmic scale to display the low-level signal. There is low level contamination due to the first order spectrum of a second star near the photometric standard, as well as three compact images, either ghosts or zeroth-order spectra of other stars in the field. The appearance of the third-order spectrum was seen to be somewhat different than expected from ground testing, with a minimum within the SUBSTRIP256 aperture that was not seen previously. It must be borne in mind that the ground testing

source was a comparatively low temperature blackbody source (T~1000K) with very little signal in third order.

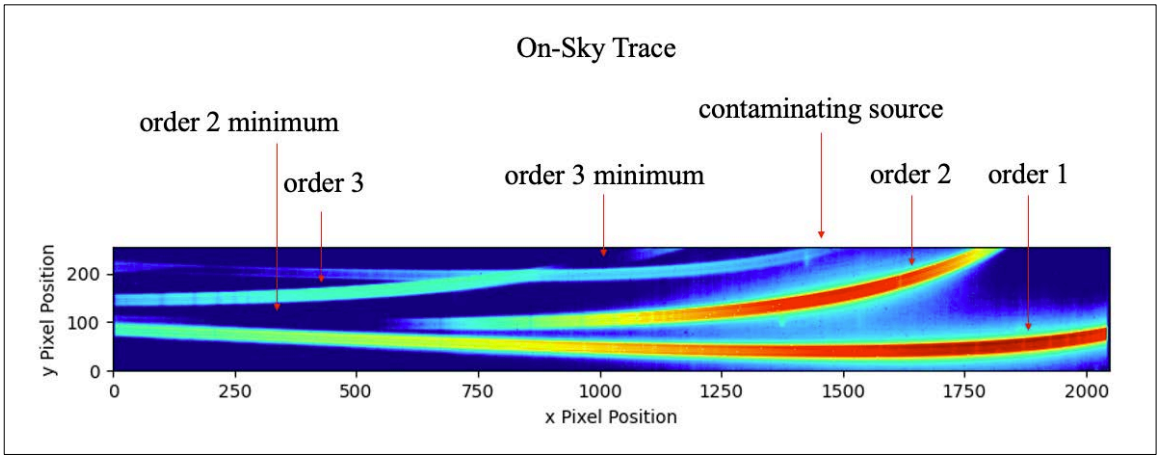

Figure 1: A display of the mean rate image from the pipeline for the GR700XD/CLEAR observation of BD+60°1753 using a logarithmic colour scale to show the low-level structure.

An examination of the Sloan Digital Sky Survey image for the area around the star using the Aladin function within APT shows the likely contaminating source. The SDSS image is shown in Figure 2. The "down" direction on the sky within the aperture shown in Figure 2 corresponds to a spectrum shifted up in the NIRISS sub-array image because of the rotation of the aperture on the sky. Similarly, the shift to the right on the sky image shown in Figure 2 produces a shift to the left in the NIRISS sub-array image. The faint galaxies to the left of the standard star in Figure 2 are too diffuse and too faint to produce measurable contamination in the rate image.

The contaminating star is identified as 2MASS 17244630+6025483 from the sky images. The contamination order 1 spectrum is about 100 times fainter than the order 1 spectrum of the standard itself. The 2MASS and Gaia DR3 data for the fainter star are consistent with it being a K5V star. According to the 2MASS catalogue the star has: J = 14.53±0.03, H = 13.87±0.04, and K = 13.69±0.05; and it is also Gaia DR3 1435897078467442432 with G = 16.3892±0.0006, G_{bp} = 17.130±0.005, and G_{rp} = 15.552±0.003. For comparison the Gaia DR3 and 2MASS photometric data for BD+60°1753 are: J = 9.612±0.022, H = 9.651±0.018, K = 9.645±0.015; the star is Gaia DR3 1435896975388228224 with G = 9.6839±0.0028, G_{bp} = 9.6884±0.0008, and G_{rp} = 9.6582±0.0004. The contaminating star has a parallax of 1.415±0.039 milli-arc-seconds, whereas the parallax measurement for BD+60°1753 is 1.782±0.056 milli-arc-seconds. There are a few other, generally much fainter, objects catalogued by Gaia in the area and seen in Figure 2. None of these seems to produce a visible spectrum on the mean rate image. There are also some faint compact "objects" in the rate image that are either due to ghost images or due to zeroth-order spectra of fainter stars, but whose cause has not been explicitly identified.

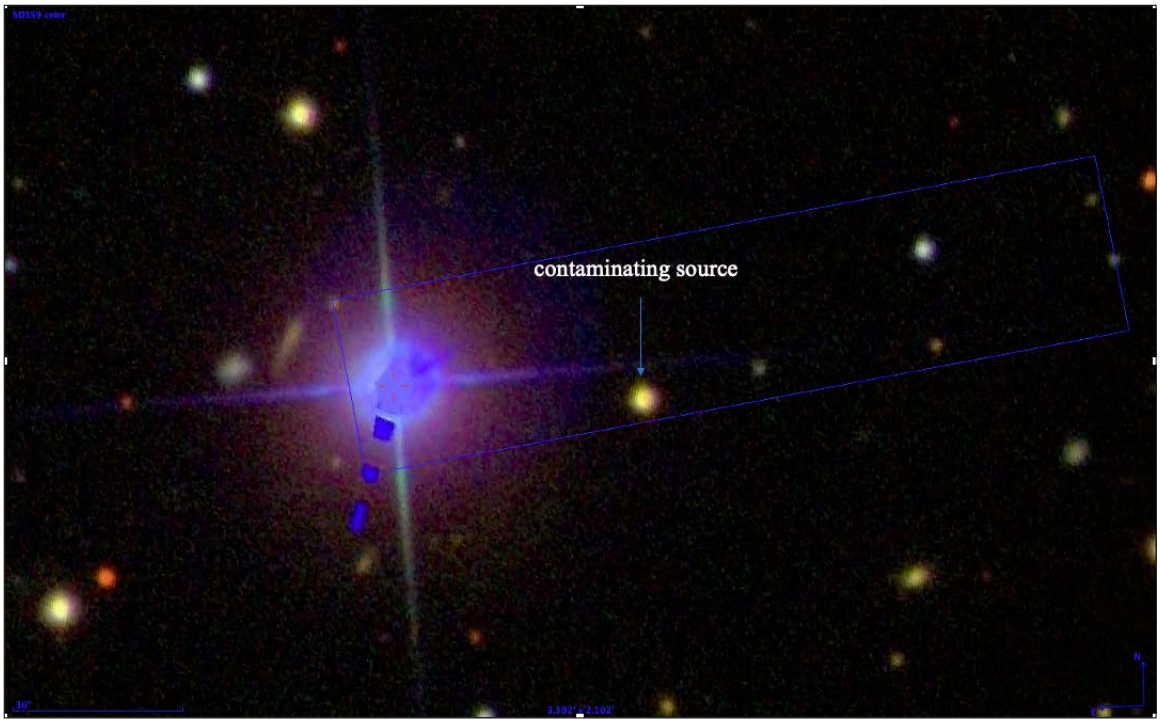

Figure 2: A view of the sky image from Aladin/SDSS with the SUBSTRIP256 sub-array projected sky position for the BD+60°1753 observation. The standard is the bright blue star, which shows some image artifacts in the SDSS image. The contaminating star is the much fainter/redder star marked on the image.

For the order 3 response curve the wavelength range where the overlap from the contaminating star occurs, which is already an area of low signal because it is close to the blaze minimum, was simply excluded from the fitting process. Given the fairly large uncertainties for this wavelength range due to the low S/N, the fitting would be of low quality even if the contamination was not present. The order 3 response function needs some improvement via changing ATOCA to extend the order 3 trace through the minimum to the shortest wavelengths covered by this mode. However, in scientific terms the order 3 extraction is a low priority because it gives redundant information already covered in order 2.

Figure 3 shows the extracted spectra. As discussed above the ATOCA extraction does not cover the full wavelength ranges of order 2 and 3, so for this plot the alternative box extraction is used to cover the entire wavelength range in second and third order. The second order spectrum after the minimum is significantly affected by the overlap with first order. The ATOCA spectrum is nearly identical to this extraction over the common wavelength range because the deblending function was not operational for the extraction. The wavelength solutions for these spectra were derived from the hydrogen absorption lines in the spectrum itself, rather than using the "official" wavelength solution derived from program APT1092. The differences in the wavelength solutions are generally small over most of the wavelength range.

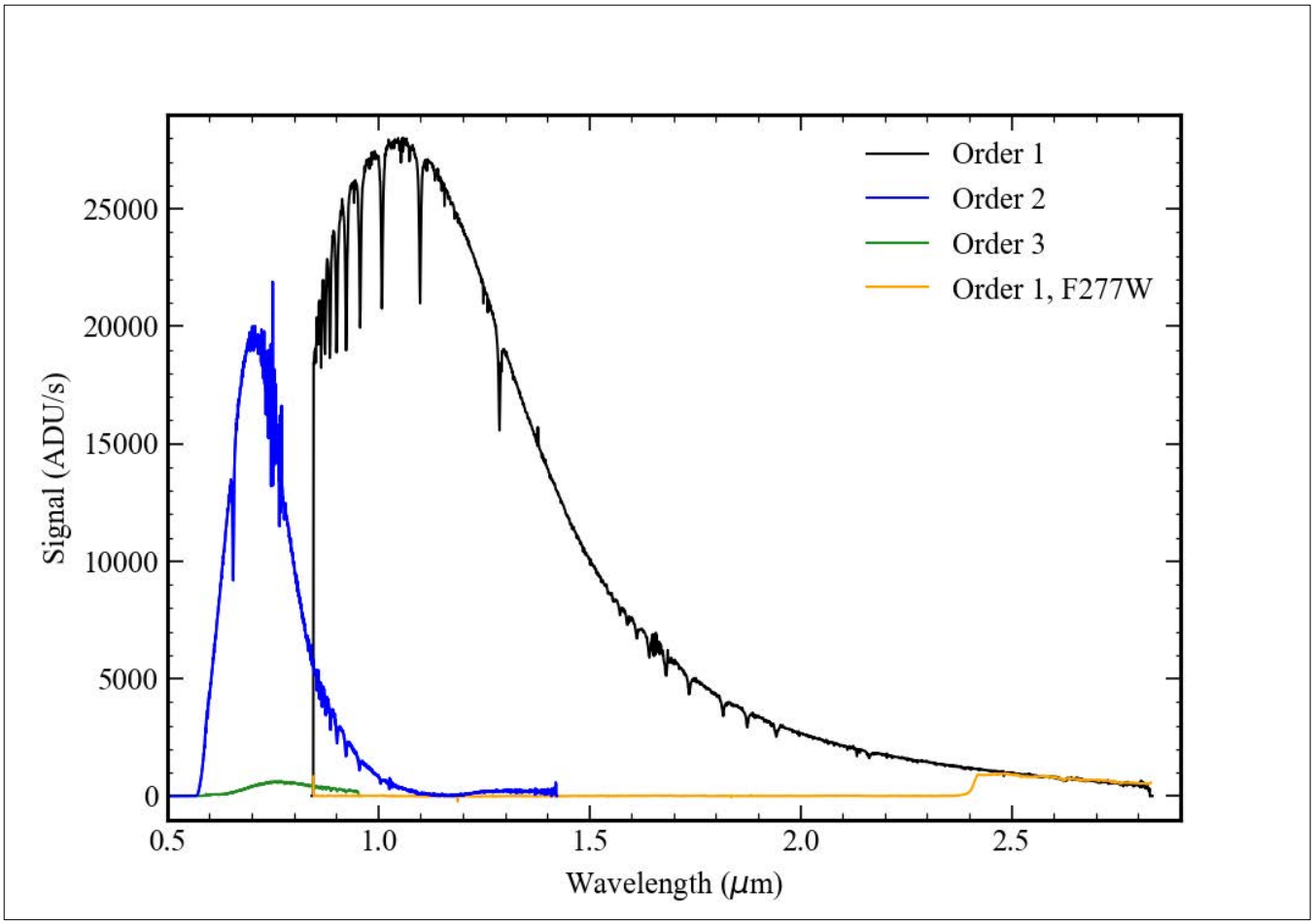

Figure 3: The extracted spectra from observation 2 of program 1091 for BD+60°1753. These spectra are from a simple box extraction with a ±20 pixel region around the trace position. The wavelength calibration is from the same observation using the hydrogen lines visible in the spectrum. The ATOCA extraction is very similar to this spectrum but is limited in the order 2 and order 3 wavelength coverage since it does not cross the spectral minima in finding the trace.

The extracted spectra were not corrected by any type of aperture correction, because for this mode estimation of the corrections is very uncertain. Unlike the imaging and Wide-Field Slitless Spectroscopy (WFSS) modes it is found that the predicted PSF from the WebbPSF program (Perrin et al., 2014) is not a very good approximation to the wings of the SOSS PSF. The observed PSF has a very board component extending at least 200 pixels to either side of the main profile at a relatively low level which is not reproduced by the WebbPSF calculations. Thus, we are not able to use WebbPSF to estimate the aperture corrections as a function of wavelength in this case. Direct estimation of the aperture corrections was not possible from either these observations or the other SOSS mode observations in commissioning, due to a combination of the usual placement of the SOSS spectrum at the upper edge of the NIRISS detector, so no measurements can be made on one side of the spectrum, of the limited number of full frame SOSS exposures, and of contamination by other sources in the single case where a

commissioning observation was made with the spectrum offset to the middle of the detector field.

For delivery of the photometric calibration files to the JWST pipeline, the as observed values were used without aperture correction; this means that the photometric calibration derived here only applies to extractions with the same ±20 pixel aperture as was used in extraction of the standard star spectrum. While this would be a problem for either imaging or WFSS modes, the hope is that SOSS mode observations will all have the star placed in the same position to a high degree of accuracy so that any aperture corrections are common to all observations. This will need to be tested with additional photometric observations in cycle 1 calibration.

4.0 Derivation of the Photometric Calibration

All the steps following the extraction of the spectra were done using code from https://github.com/spacetelescope/niriss-commissioning/tree/main/nis_comm/nis_017. The process was to run *make_sensitivity.py* to generate the sensitivity functions, then use *fit_sensitivity.py* to produce the fit functions, and then *make_reference_file.py* to bundle these into the new pipeline reference file.

The derivation of the photometric calibration factors was carried out using the extracted spectra and the CALSPEC bd60d1753_mod_004.fits stellar model. For each pixel in the extracted spectra from ATOCA the ratio of the flux density in Jansky from the standard star model to the observed count rate in ADU/s was calculated. The stellar model was smoothed to the SOSS wavelength resolution before the flux density was extracted at the different wavelengths.

The type of function produced is shown in Figure 4. Several things are apparent from this plot. First, the conversion value varies significantly over the range of wavelengths covered by the first order. This is primarily due to the blaze response of the grism with wavelength. Second, one sees variations from the mean curve whenever the spectrum crosses a spectral line, with the values going down and then up again where the Paschen series lines are seen in the spectrum. The same effect is seen for Hα in second order and for a small number of Brackett series lines visible at the long wavelength end of first order. This indicates a mis-match of the line profiles in the model spectrum with those in the NIRISS spectra. One can still trace a smooth response function by eye so excluding the points within the spectral lines should not cause any issues with the response function.

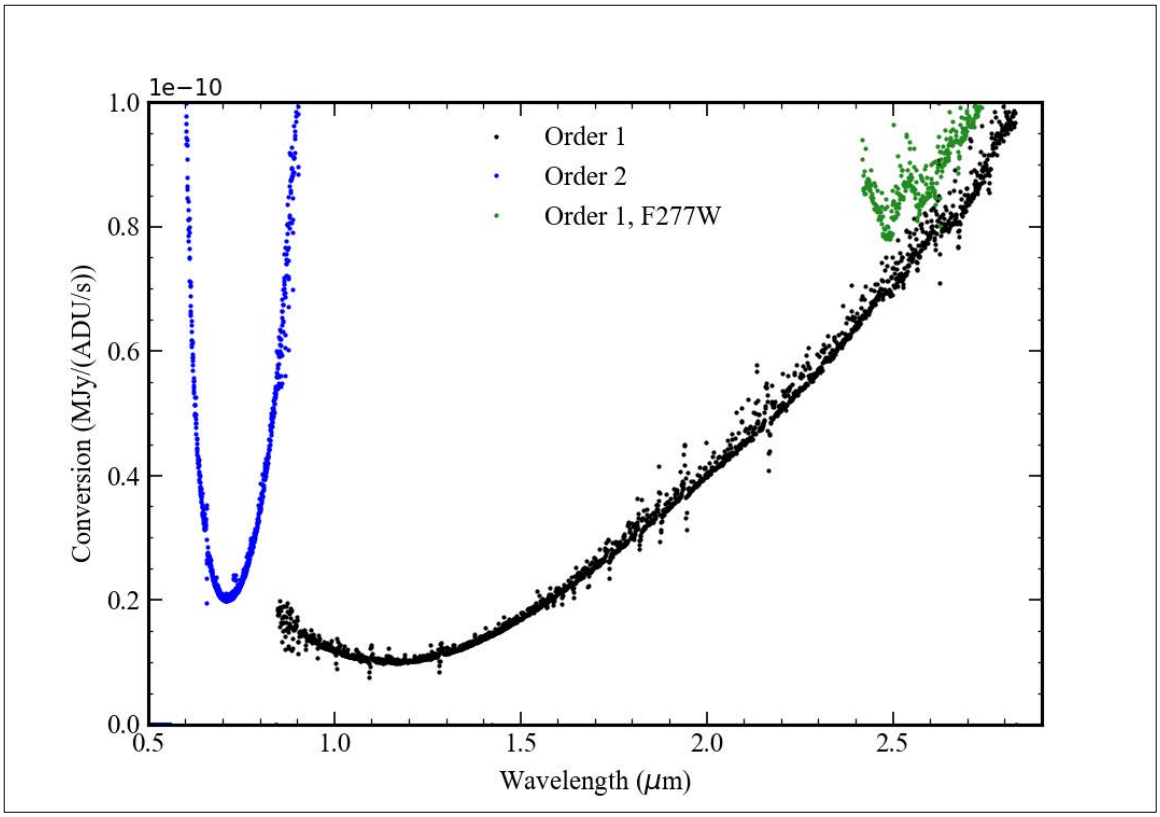

Figure 4: Conversion values calculated from the ATOCA extraction for the BD+60°1753 time series observation. Values are shown for the CLEAR orders 1 and 2 case and for the F277W order 1 case. Smaller conversion values mean better sensitivity.

One also sees a sub-set of the points with values above the general trend with wavelength, more so at the longer wavelengths. These points are cases where the box extraction is affected by a bad pixel. The pixels are masked to zero and hence reduce the total signal, which when forming the ratio raises the conversion value. Ideally this will be improved when the ATOCA software is operational. Both due to the issue with the larger values in specific columns of the image and the issues in the spectral lines, rather than using the measured values directly it is necessary to fit a smooth function to the points to produce values that can be used for the JWST pipeline.

The nature of the fitting function depended on the general shape of the conversion function. For the CLEAR case, polynomial fitting was used and the order was selected to produce a good fit over the data range and to produce a smooth extrapolation at both long and short wavelengths. For the F277W case the F277W filter imposes a sharp cut-off and produces discrete structure over the part of the response that is covered by the spectrum, so in that case a higher order spline function was used to allow the fitting function to follow the data points reasonably well. Figure 5 shows the plot with the fitting functions added as dashed lines.

The order 3 response is significantly lower than that for the other orders, and the order 3 response is not within the range of values plotted in Figure 5. Nonetheless, the same process was carried out for the CLEAR order 3 case as for orders 1 and 2.

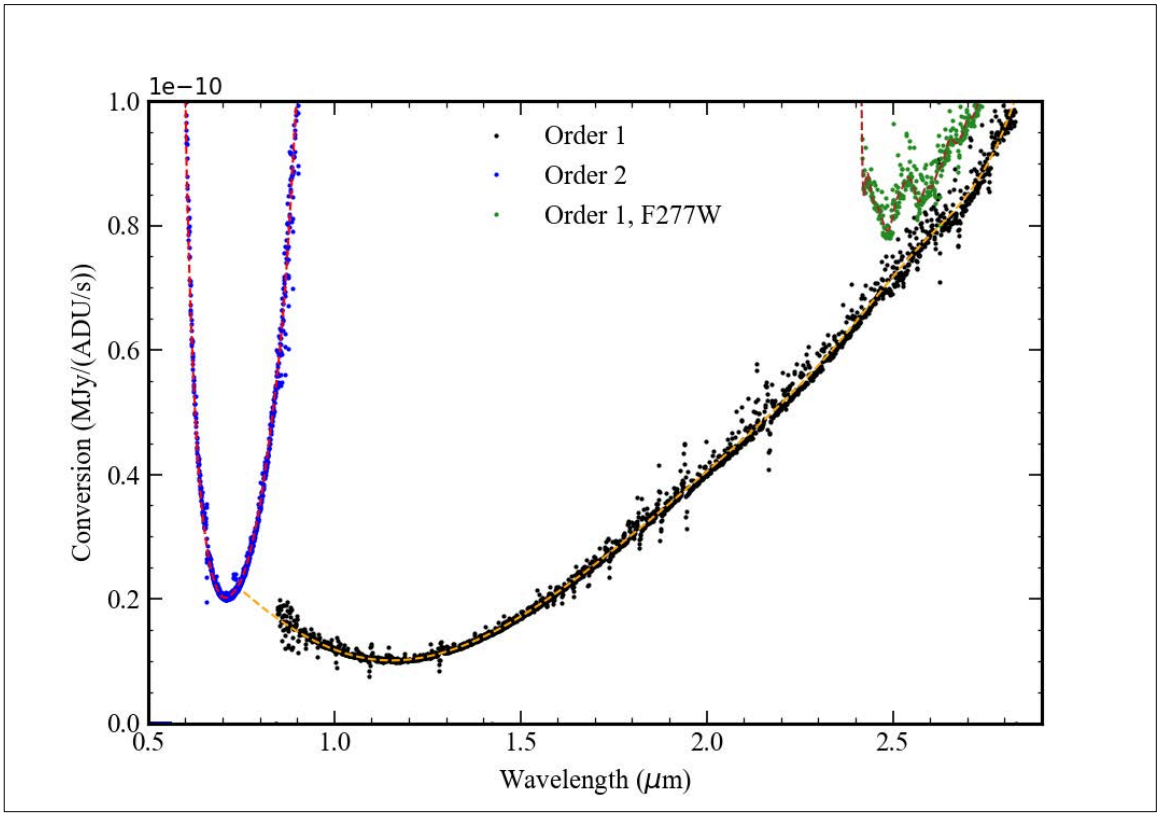

Figure 5: Conversion values calculated from the ATOCA extraction for the BD+60°1753 time series observation, with the addition of the fitting functions (dashed curves).

Once the output functions had been calculated, the four functional curves were used to create the JWST pipeline reference file for SOSS photometry. This file is specific to the extraction aperture used, and also to the extraction method used. If a SOSS spectrum were extracted with a different aperture or the extraction was changed from a simple box extraction to some other algorithm, such as optimal extraction, the values in the photometric calibration file would become invalid for the resulting spectrum and some type of correction would need to be made.

The validation of the photometric values will need to be revisited at a later date once the ATOCA extraction is working properly.

The photometric values were packaged for the pipeline and submitted to the Calibration Reference Data System on June 30th. The reference file is jwst_niriss_photom_0034.fits.

5.0 Photometric Stability

The standard star BD+60°1753 has been observed by the TESS mission, from which an estimate of the photometric stability can be found. An upper limit of 0.17%

variability peak to peak on time scales larger than 30 minutes was determined from those data (Mullally et al. 2022), which corresponds to a 1σ variation of about 0.03%. The NIRISS time series data from the second observation of program 1091 can also be used to determine the photometric stability of the star over the period of observation. The full set of 876 ramps comprises a set of measurements that can be examined for changes with time. To avoid the effects of bad pixels, any pixel with a DO_NOT_USE flag in any of the 876 rate images from the observation was masked out, along with the reference pixels. These were a bit under 2% of all the pixels in the 2040×248 illuminated area of the SUBSTRIP256 sub-array. The total signal from each masked rate image was then measured. The plot of the values normalized to the mean value (2.8788 10^7 ADU/s) is shown in Figure 6.

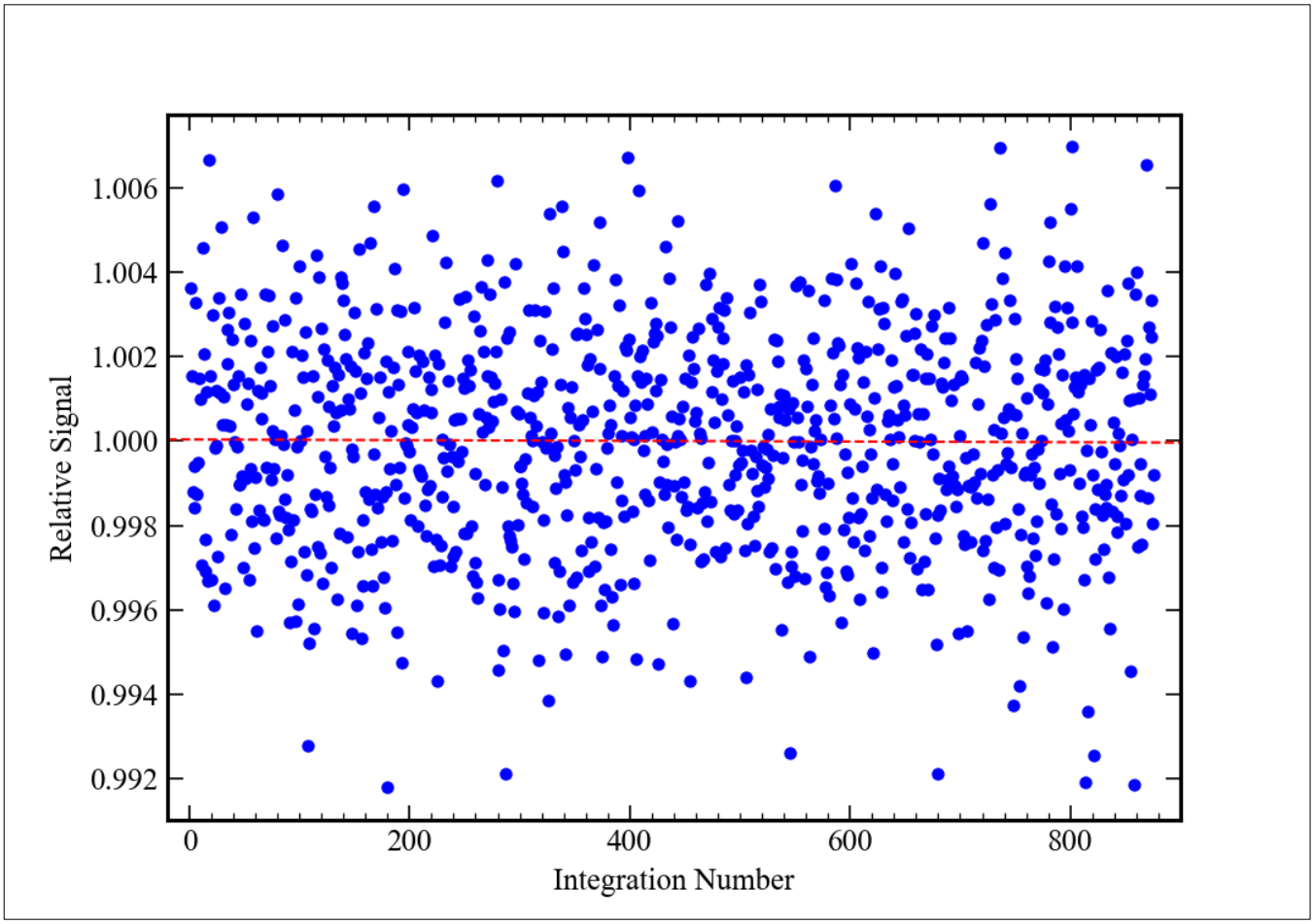

Figure 6: The integration-by-integration relative signal values from the time series observation of BD+60°1753 plotted against the ramp number. The dashed curve is the best-fit linear fit to the data points. Each integration represents about 22 seconds of clock time. The integrations are normalized to the mean signal from the set, 2.8788 10^7 ADU/s.

Looking at the distribution of the individual relative signal values shows that that histogram is approximately Gaussian with a best fit mean value of 1.000052 and a sigma value of 0.00260. The peak of the actual histogram appears to be a bit flatter than

expected for a Gaussian function, although this may be within the uncertainties from small number statistics. There is an asymmetry to smaller values at the lower edge of the distribution; the skew for the set of points is –0.144 and the kurtosis is +0.084 which indicate some asymmetry in the values. The histogram and the best fit Gaussian function are shown in Figure 7. The range is symmetric about the mean value of 1.0, but one sees a deficit of points on the high side compared to the low side of the histogram.

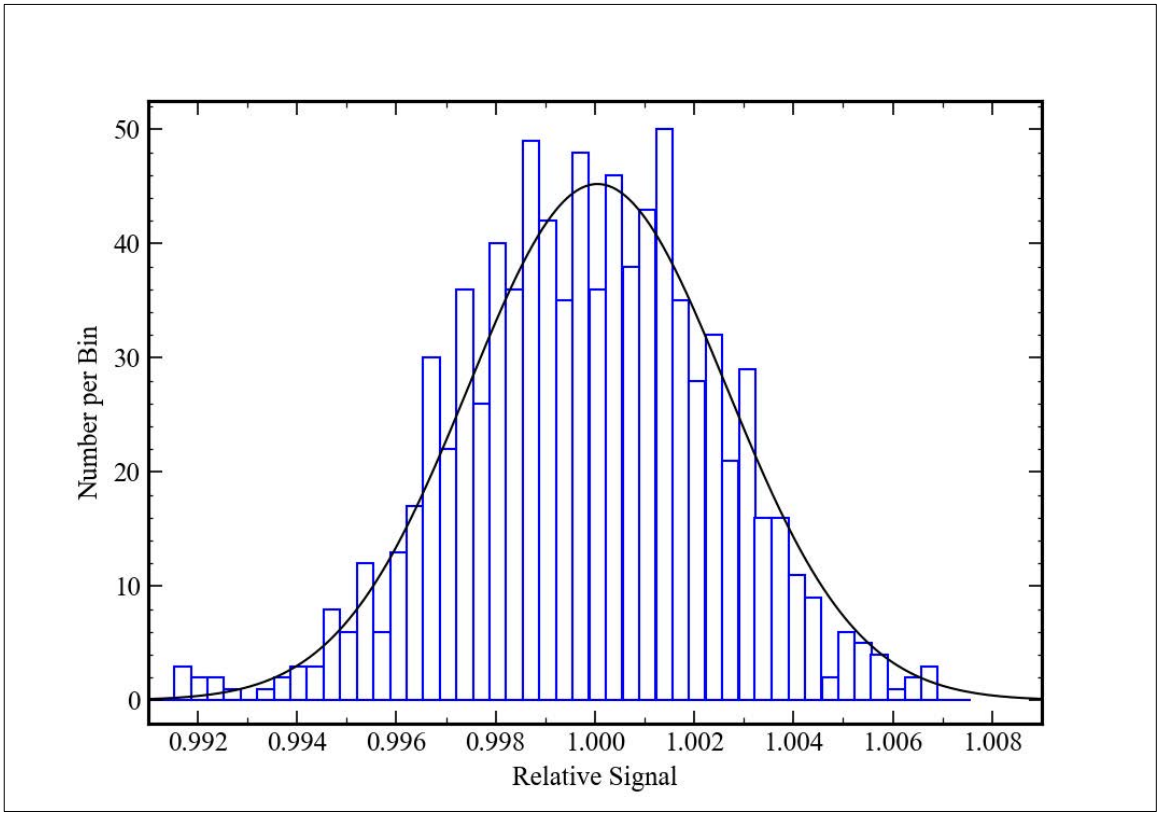

Figure 7: The histogram of the normalized integration-by-integration signal values. Also plotted is the best-fit Gaussian function.

There are various ways to test for the photometric stability. The mean signal from all the unmasked pixels was found to be 2.8788 10^7 ADU/s, with a sample standard deviation of 74000 ADU/s, a 1σ fractional uncertainty of 0.26% which an order of magnitude larger than the TESS upper limit variability value. This measurement includes the background signal which is assumed to be constant, and which is roughly 15% of the total signal in the full image although it has not been estimated for the masked rate image. The best fit trend line to the data points, shown in Figure 6, has a relative change of $-8.11\ 10^{-8}$ per integration, hence the derived total signal change over 876 integrations would be 0.007% variation over 19250 seconds. This level of variation is consistent with zero variation in the formal sense given the point-to-point scatter in the measurements, but is larger than the type of signal variations that the exoplanet transit community is interested in detecting in their analysis. It is an open question at the time of the writing of this report as to whether the variation is real and assuming that it is real whether it is due

to some small systematic effect in the observation, such as from slow changes to the telescope wavefront error causing tiny variations in the aperture corrections for the spectra, or some change within the NIRISS instrument, or whether this is due to the star. The SOSS mode is known to have some sensitivity to changes in the JWST primary mirror alignment at larger levels of change than what is derived here, as when there is a small mirror segment tilt event, and so this trend may be telling us something about the evolution of the main mirror alignment over the observation.

6.0 Conclusions

The on-orbit photometric response of the NIRISS SOSS mode was measured on-orbit in program NIS-017. Due to the difficulty of estimating the aperture correction as a function of wavelength in this mode, the photometric values are specific to the ATOCA extraction with the default aperture width of ±20 pixels from the trace position. If the extraction algorithm is revised the photometric reference file will also need to be revised.

The time series data for the standard was used to put limits on the photometric variability of BD+60°1753. A small amount of change may have been observed over the 5 hour period of observation; this might be due to some factor within JWST such as very small changes in the telescope wavefront error over the period of the observation for example, or it could be due to a small level of variability in the star itself.

7.0 References

Bohlin, R. C., Gordon, K. D., and Tremblay, P.-E., 2014, PASP, 126, 711.

Mullally, S. E., Sloan, G. C., Hermes, J. J., Kunz, M., Hambleton, K., Bohlin, R., Fleming, S. W., Gordon, K. D., Kaleida, C., and Mohamed, K., 2022, AJ, 163, 136.

Perrin, M., D., Sivaramakrishnan, A., LaJoie, C.-P., Eloit, E., Pueyo, L., Ranvindranath, S., and Alvert, L., 2014, Proc. SPIE. 9143.

Reach, W. T., Megeath, S. T., Cohen, M., Hora, J., Carey, S., Surace, J., Willner, S. P., Barmby, P., Wilson, G., Glaccum, W., Lowrance, P., Marengo, M., and Fazio, G. G., 2005, PASP, 117, 978.

Wenger, M., Ochsenbein, F., Egret, D., Dubois, P., Bonnarel, F., Borde, S., Genova, F., Jasniewicz, G., Laloe, S., Lesteven, S., and Monier, R., 2000, A&AS, 143, 9.

This work has made use of the SIMBAD database, operated at CDS, Strasbourg, France.